Scientific Research Publishing

Open Journal of Geology, 2022, 12, 907-918
https://www.scirp.org/journal/ojg
ISSN Online: 2161-7589
ISSN Print: 2161-7570

The Use of Edge Enhancement Methods and Euler Deconvolution to Estimate an Ore Deposit Depth from Gravity Data

Meriem Lghoul

Polydisciplinary Faculty, Data4Earth Laboratory, Beni-Mellal, Morocco
Email: meriem.lghoul@usms.ac.ma

How to cite this paper: Lghoul, M. (2022) The Use of Edge Enhancement Methods and Euler Deconvolution to Estimate an Ore Deposit Depth from Gravity Data. *Open Journal of Geology*, **12**, 907-918.
https://doi.org/10.4236/ojg.2022.1211043

Received: September 28, 2022
Accepted: November 13, 2022
Published: November 16, 2022

Abstract

The Hercynian massif of the central Jebilet (Morocco) is characterized by the outcrop of many gossans with great economic importance. This work focuses on interpreting gravity data of Benslimane gossan, located about thirty kilometres to the North-West of Marrakech. The residual gravity map of the study area highlights several anomalies which coincide with the mining and geological contexts. Applying edge detection methods, for example, tilt angle derivative (TDR), the total horizontal derivative of the tilt angle derivative (HDR_TDR) and the 3D Euler deconvolution, allowed us to estimate the depth of the Benslimane deposit. As a result, the average depth of the ore deposit was estimated to exceed 200 m. The results are promising, and the processing methods must be applied to the other gossan in the Jebilet massif for further exploration studies.

Keywords

Benslimane, Tilt Angle Derivative, 3D Euler Deconvolution, Depth, Total Horizontal Derivative of the Tilt Angle Derivative

1. Introduction

The Hercynian massif of Jebilet is known for its potential mining, attested by the many metalliferous deposits with great economic importance (Draa Sfar, Kettara, Koudiat Aïcha, etc.) (**Figure 1(b)**). These deposits have been the subject of many academic studies and various types of work mining exploration [1] [2]. The gossans, present in abundance at the Paleozoic massif, cover most of these deposits and constitute excellent guides for mining exploration. This type of deposit is sought to meet the needs of local industry for sulfuric acid necessary for

transforming phosphates and producing base metal ores (Zn, Cu, Pb).

Geophysics applied to mineral exploration uses principles and physical methods for discovering mineral deposits. Potential field methods (gravity, magnetic, electromagnetic) are advantageous for revealing characteristics of multi-source mineralization-related anomalies that can be further used for defining mineral exploration criteria, which could be represented quantitatively in either spatial domain or frequency domain. Therefore, data of potential field, typically in the form of sparse datasets integrated with geological datasets and other geoscience datasets, are widely applied to either 2D or 3D modelling for mineral exploration targeting. [3] analyzed the regional gravity data to locate metallic ore deposits (Burkina Fasso). [4] used large-scale gravity data to delineate iron mineralization (Rajasthan province, India). [5] used gravity data to locate Edge position and estimate depth for mineral exploration (Turkey).

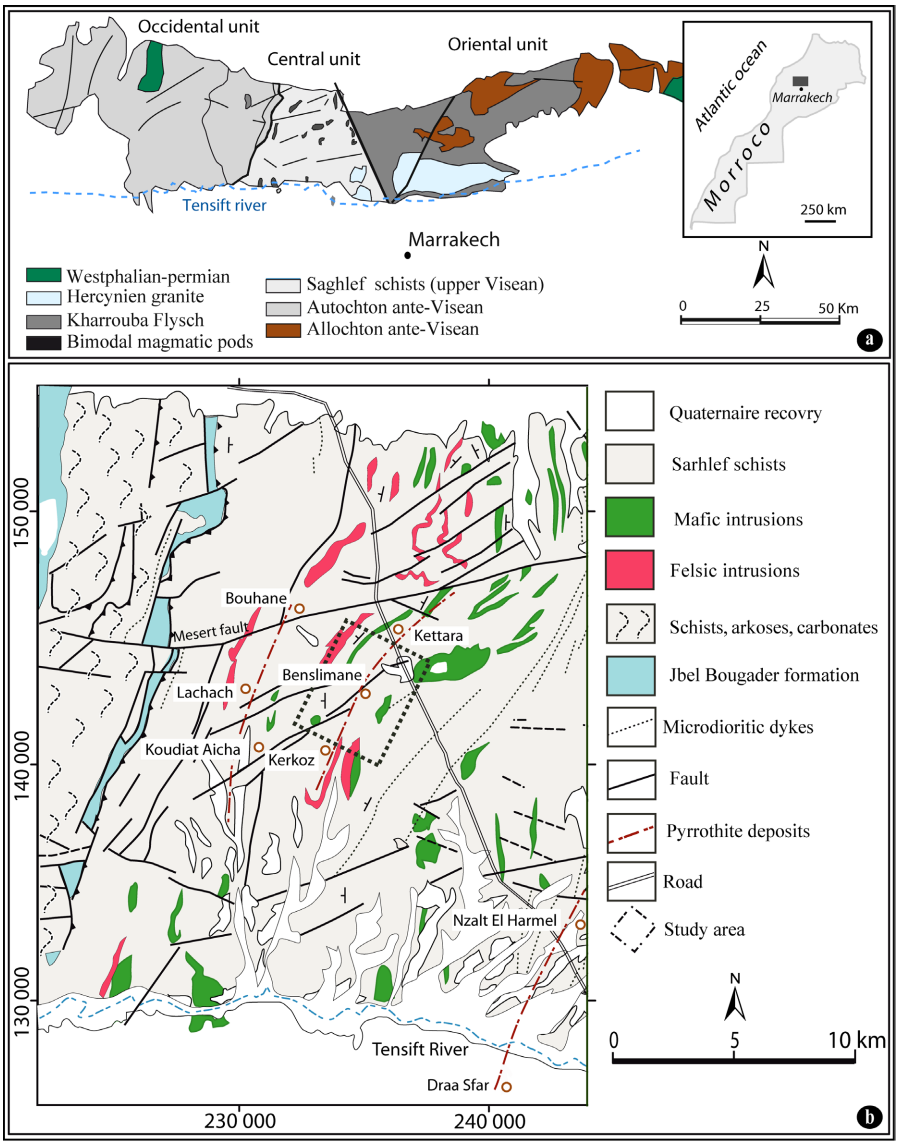

Figure 1. Regional (a) and local (b) geological map of the study area.

[6] applied gravity data to get a comprehensive geological and metallogenic model of Sn-(W) ore deposits (Central Iberian Zone, Spain). In mineral exploration, the gravity method is still widely used to identify geological context and major structures [7] [8] [9] [10] [11].

This study concerns the gossan of Benslimane. The Benslimane gossan is a sulfide deposit of Zn-Cu-Pb located at the south-eastern extension of the Kettara deposit [11]. This gossan constitutes with the Kettara in the North-East and Kerkoz in the South, one of the main lineaments of sulfide deposits of the central Jebilet massif (**Figure 1(b)**).

In this study, we interpret gravity data combined with surrounding geological information to estimate the depth of the Benslimane deposit. In this goal, the gravity data are analyzed with a qualitative approach using Bouguer anomaly, Tilt derivative, Total horizontal derivative of tilt derivative and 3D Euler deconvolution methods.

2. Geological Setting

The Hercynian massif of Jebilet is part of the western Moroccan Meseta (**Figure 1(a)**); it extends towards E-W, north of the city of Marrakech. Three major units constitute this massif: western, central and eastern, given the nature of the terrain and the style of the Hercynian tectonics that affects it [12]. The Benslimane gossan site, which is the subject of this study, belongs to the central Jebilet unit, formed mainly of a volcano-sedimentary series comprising intrusive magmatic bodies (gabbro, granite, etc.) in metapelites called "Sarhlef shist" whose age is reported to the Upper Visean-Namurian [13] (**Figure 1(b)**). The Benslimane appeared as a series of lenticular gossan in a few kilometres long.

From a structural point of view, the carboniferous formations that forme the Sarhlef serie of Central Jebilet have undergone intense Hercynian deformation. They were first affected by a major phase of synschistous folding in a sub meridian direction (N0 to N30), accompanied by a schistosity subparallel to the stratification associated with epizonal metamorphism [2]. Then, during a second phase, the central Jebilet were the seat of shears sub-parallel to the schistosity flow, they taken up by a folding associated with a crenulation schistosity. The third and last phase is characterized by conjugated dextral and sinistral strike-slip faults oriented towards N70E and N135E [12].

In mining context, the sulfide deposits are mainly polymetallic orebodies dominated by pyrrhotine and intimately linked to rhyolitic volcanism [2]. These mineralizations are consistent with the stratification of the host rocks and are often associated with underlying stockwork zones. These are volcano-sedimentary type mineralizations which are relatively distal to the volcanic manifestations contemporary with their formation [13]. At the outcrop, the sulfide mineralization is strongly oxidized and altered into limonitic products, which form gossans. The central Jebilet massif is characterized by three principal gossans lineaments (**Figure 1(b)**):

- the Koudiat Aïcha-Laachach-Bouhane lineament;
- the Kerkoz-Benslimane-Kettara lineament;
- the Draa Sfar-Nzalet El Harmel lineament.

These gossans are organized in the form of sub-meridian lineaments parallel to the Hercynian structures [13].

3. Materiel and Methods

3.1. Data

Gravity data used in this study have been obtained from the Moroccan Ministry of Mines and Energy [1]. They were acquired from April 11 to May 2, 1988. The measure stations were uniformly distributed over the study area. Data were collected using a Lacoste & Romberg gravimeter that allowed a resolution of 0.01 mGals. The gravity database contains a total of 1800 measurements. Gravity data were processed using a reduction density of 2.67 g/cm^3. The gravity data used in this study is obtained by digitalizing the Bouguer anomaly map [1]. The data are processed using Geosoft oasis montaj [14].

3.2. Methodology

- Filtering technique

Different techniques can be used to filtrate the regional component from the residual component. The Fast Fourier Transform (FFT) was applied on the gravity data for calculating the energy spectrum curves and examining the residual (shallow) and regional (deep) sources [15]. The method is based on the distribution of the frequency generated by high contrasts of density of the shallow and deep bodies. This filter is based on the cut-off frequencies that pass or reject certain frequency values and pass or reject a definite frequency band. The cut-off wavelength used to generate the residual gravity map is 500 m.

- Tilt angle derivative (TDR)

The tilt derivative (TDR) filter was introduced by [16] [17]. This filter is defined as:

$$\mathrm{TDR} = \theta = \tan^{-1}\left(\frac{\mathrm{FVD}}{\mathrm{THDR}}\right) \tag{1}$$

where THDR is the total horizontal and derivative FVD is the vertical derivative.

The variation of the tilt derivative amplitudes ranges between $-\pi/2$ and $\pi/2$ (radian) [18]. An estimation of the depth of the source can be deduced from the contours of the TDR map. The zero-contour value produced by the tilt derivative (TDR) delineates closely the edges of structures [16]. The distance between the 0 to the 45 contours of the tilt angle is equal to the depth of the top of the lineament or the half distance between −45 and 45 [18] [19].

- The total horizontal derivative of the tilt angle

The total horizontal derivative of the tilt angle produces accurate-defined maxima centered over the source's edges [17]. Total horizontal derivative of the tilt angle (THDR_TDR) provides estimation of the depth to the top of the body

source [20]. Total horizontal derivative of the tilt angle (THDR_TDR) amplitude is equal to the inverse of the depth to the top of source.

THDR_TDR is the square root of the sum of the square's TDR in the x and y directions.

$$\text{THDR of TDR} = \sqrt{\left(\frac{\partial \text{TDR}}{\partial x}\right)^2 + \left(\frac{\partial \text{TDR}}{\partial y}\right)^2} \tag{2}$$

- 3D-Euler deconvolution (ED)

The Euler deconvolution is a method based on the automatic localization and depth estimation of potential field sources field data [21] [22]. Euler deconvolution equation can be written as follow:

$$\frac{\partial f}{\partial x}(x - x_0) + \frac{\partial f}{\partial y}(y - y_0) + \frac{\partial f}{\partial z}(z - z_0) = \text{SI}(B - f) \tag{3}$$

where B is the regional field, f is the observed field at (x, y, z) location, and SI is the structural index [22]. The structural index (SI) characterizes the type of source and the rate of variation of the field amplitude with distance from the source. The base of this method is founded on solving the above equation, which has four unknowns: x_0, y_0, z_0, which represent the source position, and B.

The Euler equation's calculating process is based on window size, structural index and the grid spacing. In the current work, a grid spacing of 250 m × 250 m, a window size of 10 × 10 and a structural index of SI = 1 were adopted.

4. Results and Discussion

The gravity data's radially averaged power spectrum curve of the study area displays the regional and residual, and noise signals (**Figure 2**).

The low wavenumbers signify the deep sources (red line), and the high wavenumbers (blue line) indicate the shallow sources.

The Bouguer anomaly map (**Figure 3**) shows a lateral change of gravity values ranging from −19.5 to −15.8 mGal. The gradient is increasing of Bouguer values towards the North western part of the map.

The residual gravity map (**Figure 4**) reveals a positive (P2) elongated in the NE-SW direction. This anomaly is located in the central part of the study area and is attributed to the Benslimane gossan. In the southwestern part of this anomaly, we find another elongated positive anomaly (P6) that corresponds to the continuity of the Kerkoz gossan. In Benslimane, the gossans extend those of Kerkoz towards the North-East with offsets due to the N70˚ faults. On the North-West side of the Benslimane anomaly, a positive anomaly (P1) appears directed along a NE-SW axis and is marked by a strong gradient. It is superimposed on a band of gabbro. This band of gabbro continuously crosses the northern half of the sector; it becomes discontinuous by the series of faults affecting the sector. This discontinuity of gabbro is appeared in the positive anomaly (P8). We noted the gabbro could reach a density of 3.05 g/cm^2. A positive anomaly (P7) trending in the NW-SE direction appears in the southwestern part of the

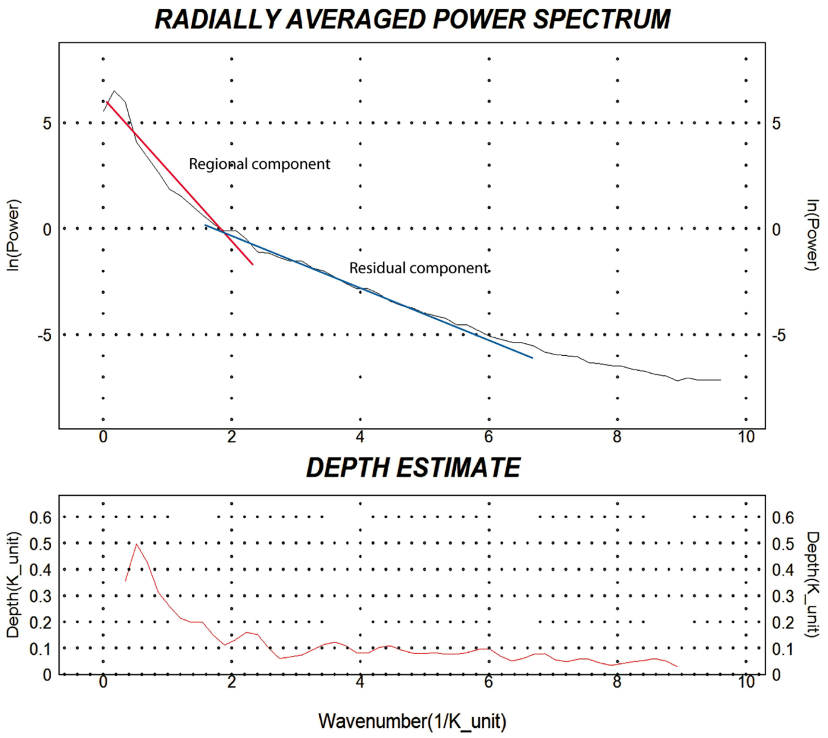

Figure 2. Power spectrum curve of the gravity data.

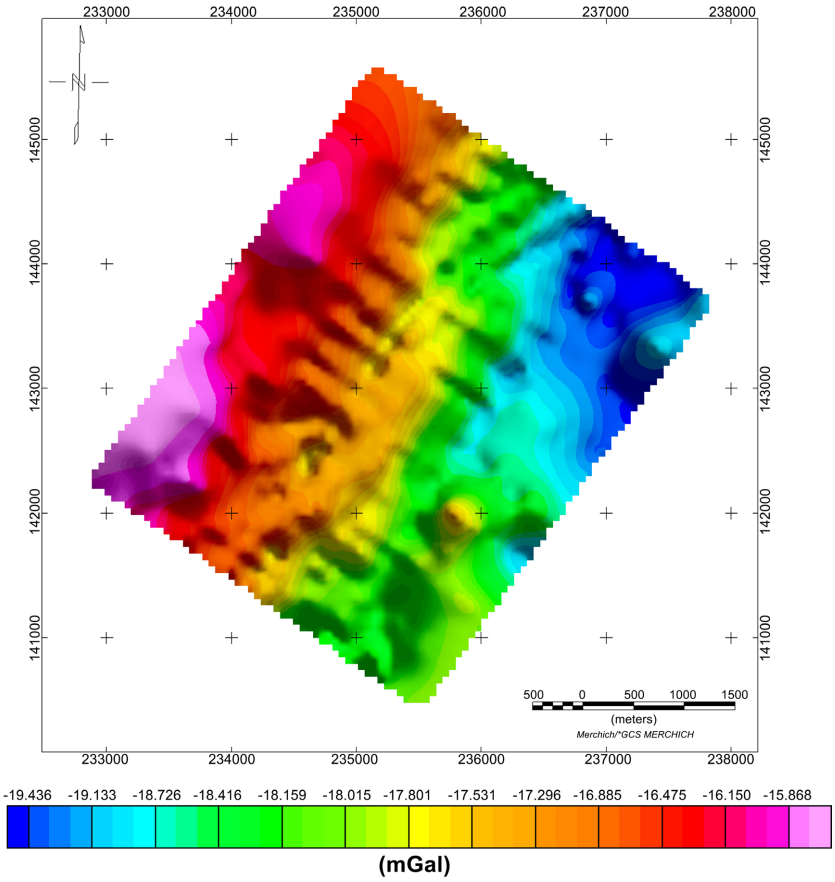

Figure 3. Bouguer anomaly map of the study area.

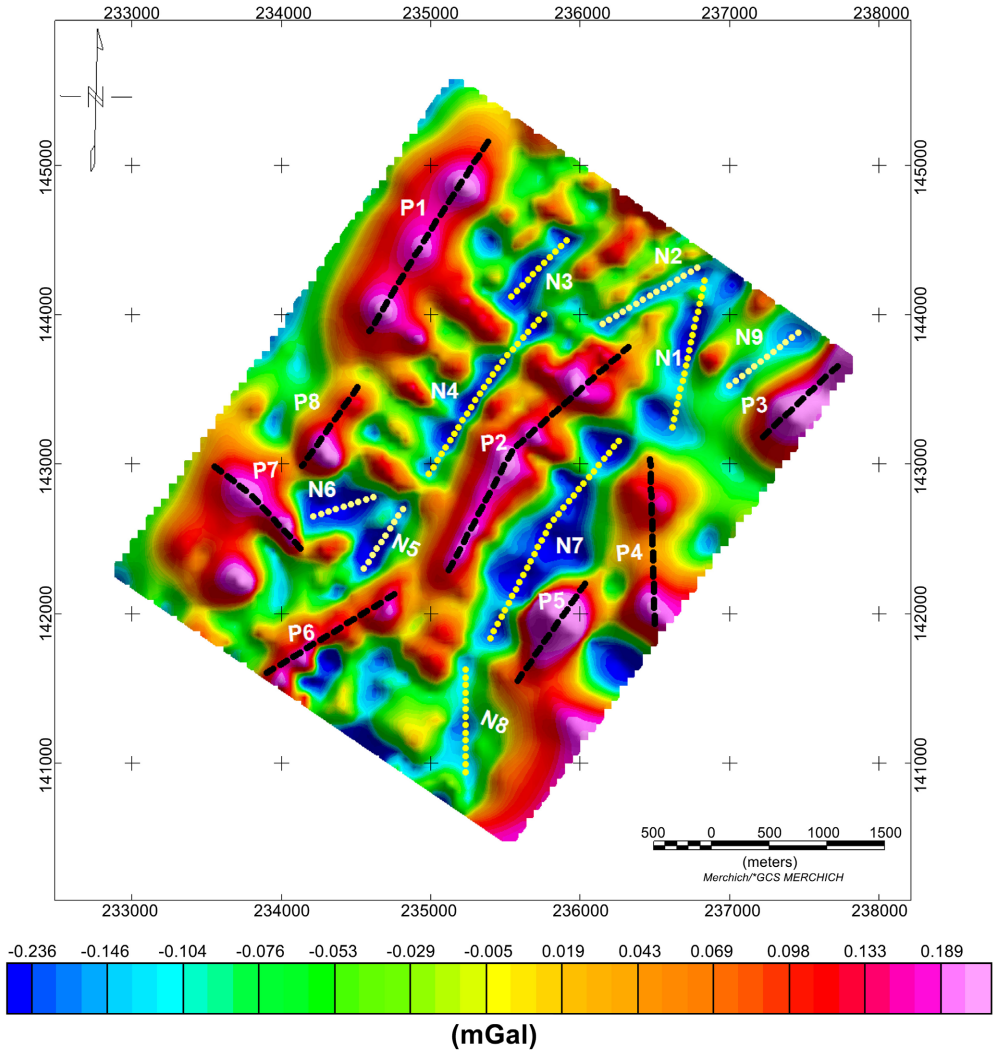

Figure 4. Residual anomaly map of the study area.

area, which can be attributed to the calcareous formation. Between the Benslimane anomaly and the previous band of gabbro, a negative anomaly (N4) trending NE-SW superimposed on passages of rhyolites.

The negative anomalies (N3) and (N5) seem to be the continuity of the rhyolite passage intersected by faults. On the eastern side of the Benslimane anomaly, we note a band of low density materialized by the negatives anomalies (N1), (N7) and (N9). This band corresponds to the felsic intrusion (rhyolites, granite).

The positive anomalies (P3), (P4) and (P5) located in the southeastern and north eastern parts correspond to gabbro intrusion. The negative anomalies (N2) and (N6) trending in the NE-SW direction correspond to the schist formation.

Figure 5 shows the tilt derivative map (TDR) map obtained from applying the filter on the Bouguer anomaly map. The contact zone between the positive anomaly and negative anomaly is well identified. This map indicates that the amplitude of tilt derivative anomalies of the Bouguer anomaly map vary from −1.361

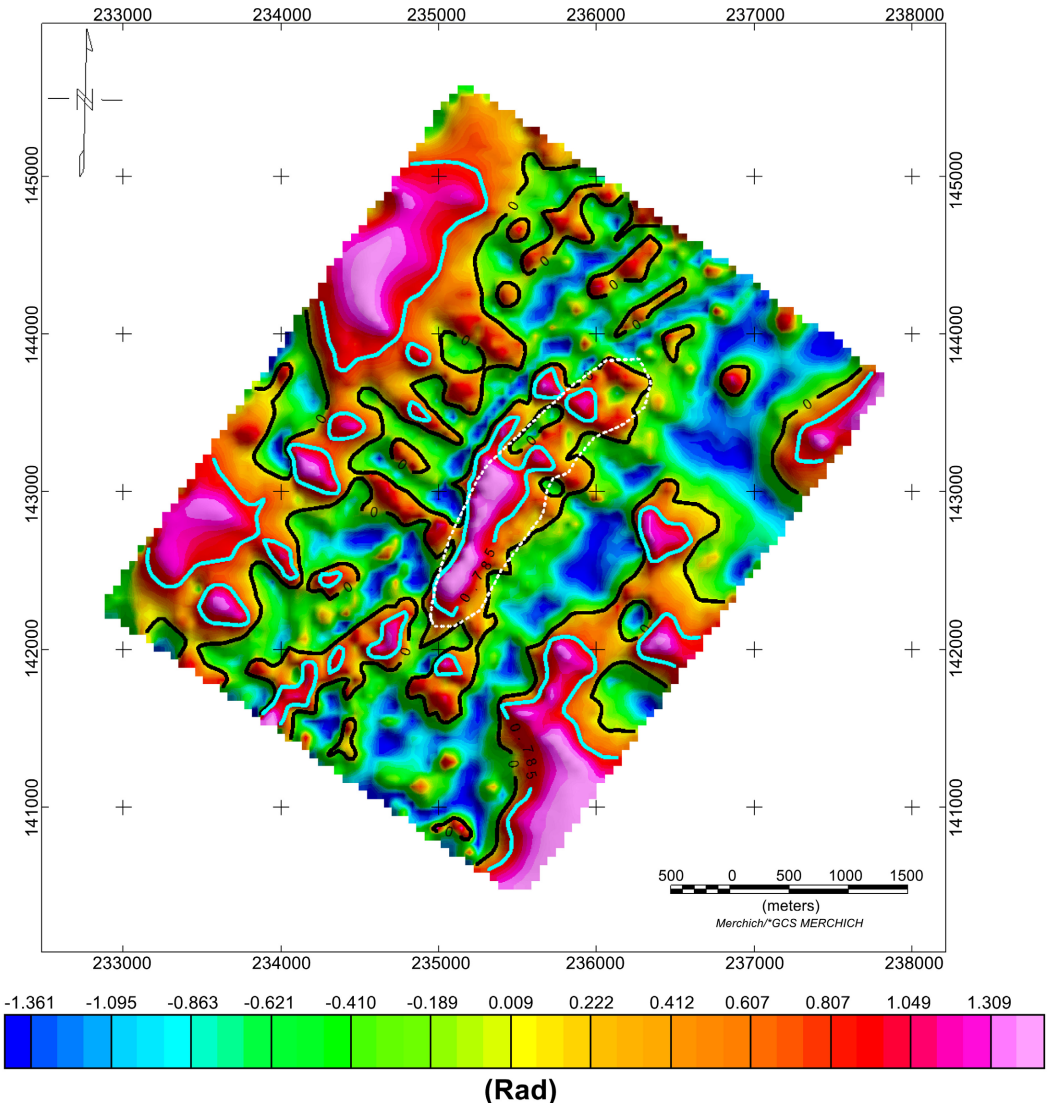

Figure 5. Tilt angle derivative map (TDR). The black line (0 rad), the cyan line (0.785). Dashed white line is the limits of Benslimane deposit.

to 1.309 rad. For the study area, the depth of the edge deduced from the distance between 0 and +0.785 radian lines shows that the northwestern, northeastern and southeastern parts have a crucial average depth that can exceed 280 m. The depth of the Benslimane gossan at the central part is about 260 m. In the north and south parts of the gossan, the depth is about 220 m and 130 m, respectively.

The THDR_TDR provide shaped anomaly with maxima over the edges of the bodies [23]. **Figure 6** shows the THDR of Tilt derivative of the Bouguer anomaly. From the colored bar scale, the depth to the top of the source ranges from 55 to about 1000 m. The estimated depth results correlate perfectly with the TDR map's results. The causatives sources bodies are deeper in the western and eastern parts of the study area and correspond to gabbro intrusion. The depth of the Benslimane deposit is about 250 m in the north part, 330 m in the central part and 142 m in the south part. For the 3D Euler deconvolution solution, a

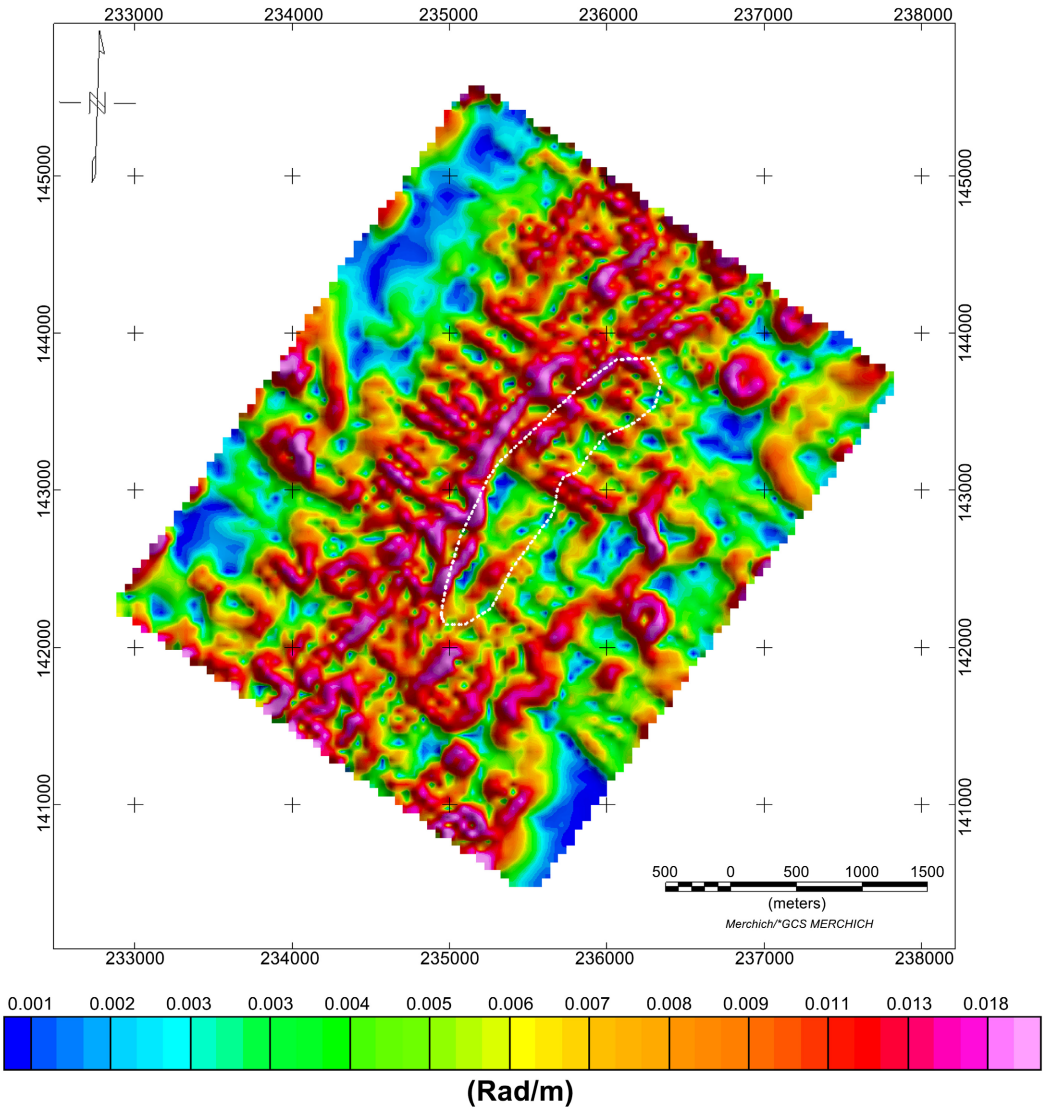

Figure 6. The total horizontal derivative of the tilt derivative (HDR_TDR) map. Dashed white line is the limits of Benslimane deposit.

good similarity with the results obtained from the previous edge detection methods is noticed (**Figure 7**). The Euler calculated depths solutions range from 80 m to 170 m. The central part of the Benslimane deposit is deeper (exceeding 170 m) than the north and south parts.

According to the Bouguer map, the Benslimane gossan and the causative structures associated with acid and basic intrusion are clearly defined. These observations confirm the relationships between the geological and mining context with the various gravity anomalies. The correlation between the gabbro of this region and the positive residual anomalies suggests that this formation has a strong gravimetric marker on the whole sector. The same is true for rhyolite which reflects a negative trait due to its low density. And finally, we observe the correlation between the surface mineralization indices (gossan) and the positive residual anomaly known as Benslimane. The enhanced methods show that the

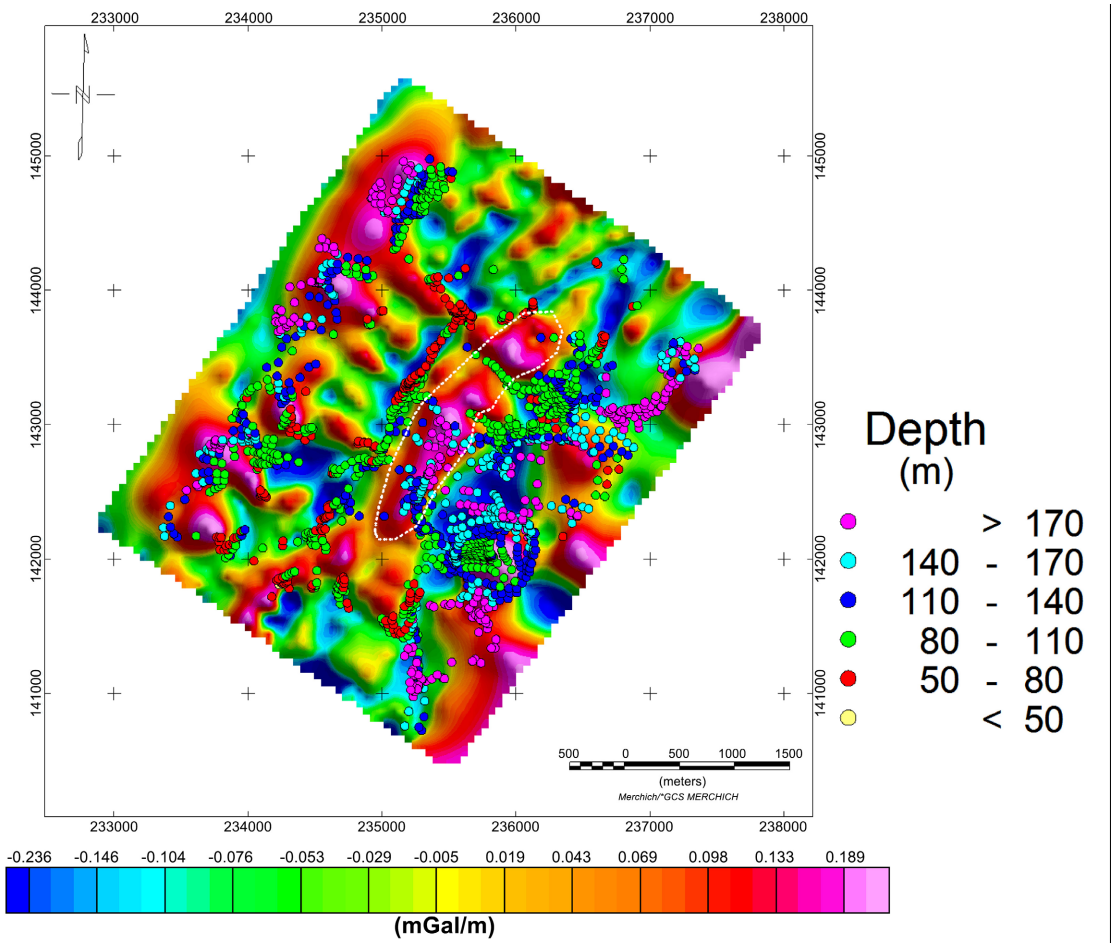

Figure 7. 3D Euler solution plotted on the residual gravity map. Dashed white line is the limits of Benslimane deposit.

causative structures in the study area's eastern and western parts, corresponding to the gabbro intrusion, are more profound. In contrast, the rhyolitic bands have a low depth. The Benslimane gossan bounded by this felsic and mafic intrusion presents an average depth of about 200 m.

5. Conclusion

Gravity data interpretation has helped map geological features and the mineralized zones within the study area. The interpretation also reveals the existence of numerous intrusive bodies. Using edge detection techniques allowed us to estimate the average depth of the ore deposit. The tilt derivative methods show that the average depth of Benslimane gossan is about 230 m. The low deeper part corresponds to the rhyolite bands, whereas the deeper part corresponds to gabbro intrusion bounded the study area in the eastern and western parts. The horizontal derivative of the tilt derivative correlates perfectly with the results obtained by the tilt derivative and shows that the Benslimane deposit has an average depth exceeding 200 m. The Euler deconvolution satisfactorily estimates the depth of the Benslimane gossan and shows an excellent correlation between the

Tilt derivative (TDR) and the HDR_tilt results. Edge detection methods from gravity data are powerful for estimating ore depth deposit; it provides a reduction in exploration time and costs. For further study, a modelling and inversion process of the Benslimane anomaly is recommended for getting an accurate idea of the geometry of the ore body.

Acknowledgements

The author is grateful to the anonymous reviewers and the editors for their constructive comments.

Conflicts of Interest

The author declares no conflicts of interest regarding the publication of this paper.

References

[1] Hathouti, M. (1990) Etude gravimétrique et magnétique des amas sulfurés viséens de la région de Marrakech. PhD Thesis, Université des sciences et techniques du Languedoc, Centre géologique et géophysique, Montpellier, 206 p.

[2] Essaïfi, A. and Hibti, M. (2008) The Hydrothermal System of Central Jebilets (Variscan Belt, Morocco): A Genetic Association between Bimodal Plutonism and Massive Sulphide Deposits? *Journal of African Earth Sciences*, **50**, 188-203. https://doi.org/10.1016/j.jafrearsci.2007.09.012

[3] Mickus, K. (2007) Regional Gravity Analysis of Burkina Faso: Implications for the Location of Metallic Ore Deposits. *Journal of African Earth Sciences*, **50**, 55-66. https://doi.org/10.1016/j.jafrearsci.2007.09.016

[4] Sahoo, S., Singh, A., Biswas, S. and Sharma, S.P. (2021) 3D Subsurface Characterization of Banded Iron Formation Mineralization Using Large-Scale Gravity Data: A Case Study in Parts of Bharatpur, Dausa and Karauli Districts of Rajasthan, India. *Natural Resources Research*, **30**, 3121-3138. https://doi.org/10.1007/s11053-021-09880-y

[5] Elmas, A. (2019) Edge Position Detection and Depth Estimation from Gravity Data with Application to Mineral Exploration. *Carbonates and Evaporites*, **34**, 189-196. https://doi.org/10.1007/s13146-018-0480-8

[6] Chicharro, E., Martín-Crespo, T., Gómez-Ortiz, D., Lopez-Garcia, J.A., Oyarzun, R. and Villaseca, C. (2015) Geology and Gravity Modeling of the Logrosán Sn-(W) Ore Deposits (Central Iberian Zone, Spain). *Ore Geology Review*, **65**, 294-307. https://doi.org/10.1016/j.oregeorev.2014.10.005

[7] Afshar, A., Norouzi, G.H., Moradzadeh, A. and Riahi, M.A. (2018) Application of Magnetic and Gravity Methods to the Exploration of Sodium Sulfate Deposits, Case Study: Garmab Mine, Semnan, Iran. *Journal of Applied Geophysics*, **159**, 586-596. https://doi.org/10.1016/j.jappgeo.2018.10.003

[8] Ysbaa, S., Haddouche, O., Boutaleb, A., Chemam, M. and Sadaoui, M. (2019) Mineral Deposits of Northeastern Algeria (Southern Medjerda Mounts and Diapiric Zone): Regional-Scale Structural Controls, Spatial Distribution, and Importance of Geophysical Lineaments. *Arabian Journal of Geosciences*, **12**, Article No. 482. https://doi.org/10.1007/s12517-019-4611-x

[9] Guo, L., Chen, Y. and Zhao, B. (2021) Application of Singular Value Decomposition

(SVD) to the Extraction of Gravity Anomalies Associated with Ag-Pb-Zn-W Polymetallic Mineralization in the Bozhushan Ore Field, Southwestern China. *Journal of Earth Sciences*, **32**, 310-317. https://doi.org/10.1007/s12583-020-1352-4

[10] Kheyrollahi, H., Alinia, F. and Ghods, A. (2021) Regional Magnetic and Gravity Structures and Distribution of Mineral Deposits in Central Iran: Implications for Mineral Exploration. *Journal of Asian Earth Sciences*, **217**, Article ID: 104828. https://doi.org/10.1016/j.jseaes.2021.104828

[11] Shirazy, A., Shirazi, A., Nazerian, H., Khayer, K. and Hezarkhani, A. (2021) Geophysical Study: Estimation of Deposit Depth Using Gravimetric Data and Euler Method (Jalalabad Iron Mine, Kerman Province of IRAN). *Open Journal of Geology*, **11**, 340-355. https://doi.org/10.4236/ojg.2021.118018

[12] Huvelin, P. (1977) Etude géologique et gîtologique du massif hercynien des Jebilet (Maroc Occidental), 232 bis. Note et Mémoires du Service Géologique du Maroc, 307.

[13] Bernard, A.J., Maïer, O.W. and Mellal, A. (1988) Aperçu sur les amas sulfurés massifs des Hercynides marocaines. *Mineralium Deposita*, **23**, 104-144. https://doi.org/10.1007/BF00206659

[14] Geosoft Oasis Montaj (2007) Mapping and Application System Inc, Suite 500, Richmond St. West Toronto, ON Canada N5SIV6.

[15] Spector, A. and Grant, F. (1970) Statistical Models for Interpreting Aeromagnetic Data. *Geophysics*, **35**, 293-302. https://doi.org/10.1190/1.1440092

[16] Miller, H.G. and Singh, V. (1994) Potential Field Tilt a New Concept for Location of Potential Sources. *Applied Geophysics*, **32**, 213-217. https://doi.org/10.1016/0926-9851(94)90022-1

[17] Verduzco, B.J.D., Fairhead, C.M., Green, C.M. and MacKenzie, C. (2004) New Insights into Magnetic Derivatives for Structural Mapping. *The Leading Edge*, **23**, 116-119. https://doi.org/10.1190/1.1651454

[18] Salem, A., Williams, S., Fairhead, D., Smith, R. and Ravat, D. (2008) Interpretation of Magnetic Data Using Tilt-Angle Derivatives. *Geophysics*, **73**, L1-L10. https://doi.org/10.1190/1.2799992

[19] Hinze, W.J., Von Frese, R.R.B. and Saad, A.H. (2013) Gravity and Magnetic Exploration Principles, Practices, and Applications. Cambridge University Press, New York. https://doi.org/10.1017/CBO9780511843129

[20] Al-Badani, M.A. and Al-Wathaf, Y.M. (2018) Using the Aeromagnetic Data for Mapping the Basement Depth and Contact Locations, at Southern Part of Tihamah Region, Western Yemen. *Egyptian Journal of Petroleum*, **27**, 485-495. https://doi.org/10.1016/j.ejpe.2017.07.015

[21] Thompson, D.T. (1982) EULDPH: A New Technique for Making Computer Assisted Depth Estimates from Magnetic Data. *Geophysics*, **47**, 31-37. https://doi.org/10.1190/1.1441278

[22] Reid, A.B., Allsop, J.M., Granser, H., Millett, A.J. and Somerton, I.W. (1990) Magnetic Interpretation in Three Dimensions Using Euler Deconvolution. *Geophysics*, **55**, 80-91. https://doi.org/10.1190/1.1442774

[23] Fairhead, J.D., Mackenzie, C., Green, C.M. and Verduzco, B.J.D. (2004) A New Set of Magnetic Field Derivatives for Mapping Mineral Prospects: A New Set of Magnetic Field Derivatives for Mapping Mineral Prospects. *ASEG Extended Abstracts*, **2004**, 1-4. https://doi.org/10.1071/ASEG2004ab042